



Additive manufacturing of multi-material parts – Design guidelines for manufacturing of 316L/CuCrZr in laser powder bed fusion

Ina Meyer^{*}, Marcus Oel, Tobias Ehlers, Roland Lachmayer

Institute of Product Development (IPeG), Gottfried Wilhelm Leibniz Universität Hannover, An der Universität 1, 30823 Garbsen, Germany

ARTICLE INFO

Keywords:

Multi-material additive manufacturing (MMAM)
Laser powder bed fusion (PBF-LB)
Effect-engineering
Process chain
Design guidelines

ABSTRACT

Additive manufacturing (AM) can be used to produce multi-material parts in which the material can be varied voxel-wise in all three spatial directions. This means that the paradigm of the homogeneous material can be abandoned and local effects such as heat conduction or damping can be selectively adjusted in the part. Recently, continuous development of machine technology has allowed the production of multi-metal materials in laser powder bed fusion (PBF-LB/MM). Compared to other additive manufacturing processes for multi-material production, this allows greater design freedom and detail accuracy to be realized. However, due to the novel character of multi-material manufacturing in PBF-LB, the process knowledge for successful and reproducible fabrication is currently lacking. This paper focuses on establishing design guidelines for manufacturing the material pairing of stainless steel 316L (1.4404) and copper alloy CuCrZr (CW106C). The article is accompanied by the development of a specific process chain. As a result of this work, design guidelines for multi-material parts are available for the first time, in regard to arrangement, size, overhangs, economy, powder quality and laser scanning.

1. Introduction

In recent decades, the technical, ecological and economic demands placed on parts have gradually increased. In order to keep up with international competition, new solutions must therefore be continuously developed. Additive manufacturing (AM), in particular the laser powder bed fusion of metals (PBF-LB/M) process, can be used to produce parts with a high degree of design freedom [1–4]. This opens up completely new design potential in product development. However, not all potentials can be fully exploited for additive manufacturing (AM) of mono-materials. Up until now, research has mainly focused on the lightweight design of topology- and shape-optimized structural parts that exhibit high potential for automotive and aerospace applications [4–6]. The design objectives of material savings, thin walls and net-shape geometries are primarily addressed. In addition to the macroscopic design parameters such as topology or shape, however, the microscopic design parameters, in particular the material properties, also have a crucial impact on the part performance [7,8]. Due to the advancing technology development of multi-material design, it is now possible to leave the paradigm of the homogeneous material, rapidly enabling new design possibilities to be realized. As a result, the design objectives of local property adjustment and internal effects can be addressed to a more significant extent. Through the additional utilization of functional materials, which are primarily characterized by their thermal, electrical, magnetic, or damping properties, it is possible to

^{*} Corresponding author.

E-mail address: meyer@ipeg.uni-hannover.de (I. Meyer).

realize technologically contradictory properties, such as high stiffness coupled with high damping or local regions containing conductive and non-conductive materials, respectively, in a single part [9–11]. By integrating various effects such as thermal conduction or damping, parts can be optimally adapted to their specific environmental conditions. This approach is also known as effect-engineering [12].

In this context, the technology of 3D multi-material parts is a crucial factor in order to adjust the materials or properties in a part voxel-wise in all three spatial directions [13–15]. In addition to well-established methods for multi-metal additive manufacturing, such as directed energy deposition (DED), there now exists the possibility to manufacture such parts in PBF-LB [12]. Compared to directed energy deposition (DED), the PBF-LB process has the advantage of being able to achieve greater accuracy and design freedom due to the smaller laser spot diameter [7,16,17]. Multi-material fabrication of metals has been used for centuries in a variety of applications in order to locally adapt properties specific to the requirements. However, the use of additively manufactured metal multi-materials has only been a subject of discussion since 1998 [18]. The technical implementation of controlled voxel-wise material placement within a material layer is currently a particularly challenging task [19,20]. So far, predominantly cuboidal 2D multi-material specimens, which exhibit a variation in material in the build direction, have been investigated [13,14,21–23]. A common finding of the results is that a strong connection between dissimilar metal/metal interfaces could be identified. However, these findings are not directly transferable to 3D multi-material parts, which offer a greater potential due to the high degree of design freedom. The technological maturity of 3D multi-material manufacturing using PBF-LB was assessed using manufacturing readiness levels (MRL) following a ten-point scale with a maturity level of four to five [24]. This indicates that the proof-of-concept of this technology has been completed and that it is already possible to produce multi-material components in a laboratory setting. By contrast, the industrial application of this technology is not yet mature [25]. On the one hand, the reasons for this are the high manual effort required for the design and data preparation of multi-material components, since no specialized design tools are available, and on the other hand, the lack of knowledge in the field of process technology [9,17,24,26–28]. In literature, there is a complete lack of recommended actions and design guidelines for the design of additively manufactured multi-materials with the aim of ensuring a reproducible manufacturing process of multi-material components and gaining control over component quality [3,7,9,24].

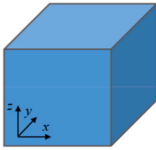
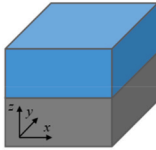
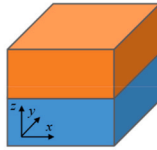
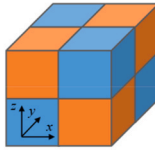
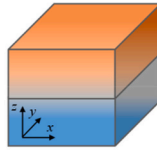
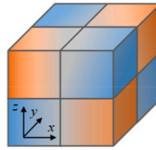
In this paper, design guidelines are developed as a supporting tool for the successful manufacturing of laser beam melted multi-material components. For this purpose, Chapter 2 identifies the challenges and potentials for multi-material manufacturing along a specific process chain. For the specific implementation of multi-material design, selected characteristic features are produced and analyzed on the basis of the boundary conditions from Chapter 3. The results are then summarized in the form of a design catalog (Chapter 4). Finally, the summary and outlook are provided (Chapter 5). This work will thus lay the foundation for establishing a set of rules for the development of laser beam melted multi-material parts.

2. Review

For a clear differentiation of the terms, this chapter first addresses the definition and structure of additively manufactured multi-material parts. In addition, the current state of research in multi-material manufacturing is outlined on the basis of the entire PBF-LB/MM process chain.

2.1. Definition of terms and classification of multi-material parts

The term multi-material is used to describe a composite of at least two microscopically definable and distinguishable materials. The materials used can belong to the same or to different material groups, such as metals, polymers, ceramics or glass. In the field of additive manufacturing, multi-material parts can be divided into categories according to the type of material transition, geometric

Mono-Material	Hybrid-Material	Multi-Material			
Homogeneous	Discrete	Discrete		Graded	
		2D	3D	2D	3D
					
No material transition	Discrete material transition in one dimension	Discrete material transition in one dimension	Discrete material transition in at least two dimensions	Continuous material transition in one dimension	Continuous material transition in at least two dimensions
Material produced by additive manufacturing	Substrate produced by conventional manufacturing	All materials produced by additive manufacturing			

■ Substrate ■ Material A ■ Material B

Fig. 1. Classification of material transitions with respect to geometric dimensions.

dimensions and manufacturing method. Fig. 1 shows a gradation between a mono-material (one material), hybrid-material (two materials) and multi-material (at least two materials) with exemplary models. Here, the three-dimensional machine coordinate system defined according to ISO/ASTM 52921 is used, where the x-y plane represents the parallel plane to the build platform and the z-axis represents the build direction of the layers [29]. In the case of the hybrid part, the substrate part is manufactured conventionally and the second material is additively built up on it. In contrast, in the case of the multi-material part, all materials are manufactured using additive manufacturing (AM). This approach finds agreement with, among others, Anstaett et al. [30] and Schneck et al. [24]. There are some discrepancies in literature regarding the assignment of the dimensions. For example, the term 1D is interpreted as either “no material change” [31] or “one material change” [25,32]. Furthermore, the term 2D hybrid has a double designation. Since the designations for mono-material and hybrid material are clearly defined, only for multi-material are the dimensions of the material transitions of 2D (material transition in one dimension) and 3D parts (material transitions in at least two dimensions) considered. Furthermore, the material transitions are categorized into discrete (clearly microscopically definable boundary) and graded (continuous boundary).

2.2. PBF-LB process chain for multi-material manufacturing and current research activities

Due to the advancing technology of additive manufacturing (AM) of multi-materials, the product development process must also be adapted accordingly. For example, additional considerations such as the selection of design tools, the definition of respective process parameters, as well as used powder recycling and post-processing strategies must be taken into account. Therefore, in the following, the holistic PBF-LB/MM process chain will be discussed in greater detail, which, like the conventional mono-material process chain, can be divided into the phases of design, pre-process, in-process, post-process and finishing (see Fig. 2) [1].

2.2.1. Design

In addition to the actual part modeling, the design process includes a large number of other steps such as planning, material selection, optimization and the determination of suitable process parameters. In the best case, most of the knowledge concerning the entire process chain must already be available in this phase, as the influence on the product development process is the most significant here.

The design process begins with the specification of requirements and the identification of design objectives. Depending on the desired technical properties, the four material groups metal/metal, metal/ceramic, metal/polymer and metal/glass can be chosen in the next step “material selection” for multi-material production in general. Special focus is currently being placed on the first material group, metal/metal. Due to the fact that the materials are similar in their properties such as atomic bonding and coefficient of thermal expansion compared to the other material groups, the joining zone results in a better bond [28]. Research by Schneck et al. [24] suggests that in hybrid fabrication, predominantly similar metals, such as two iron or aluminum alloys are investigated. In contrast, 2D multi-material manufacturing mainly uses iron and aluminum alloys with dissimilar materials, and 3D multi-material manufacturing mainly uses steel/copper combinations, such as 316L/CuSn10 [19] or 1.2709/CW106C [30]. Some materials, such as titanium alloys, are entirely absent in the research of multi-materials using PBF-LB [24]. In principle, it is useful to use aids for material selection [28, 33]. These include, for example, general methods for the selection of additively manufactured multi-materials [27], methods for the resolution of conflicting targets [34], manufacturing-specific material databases [35], and alloy compatibility charts [3].

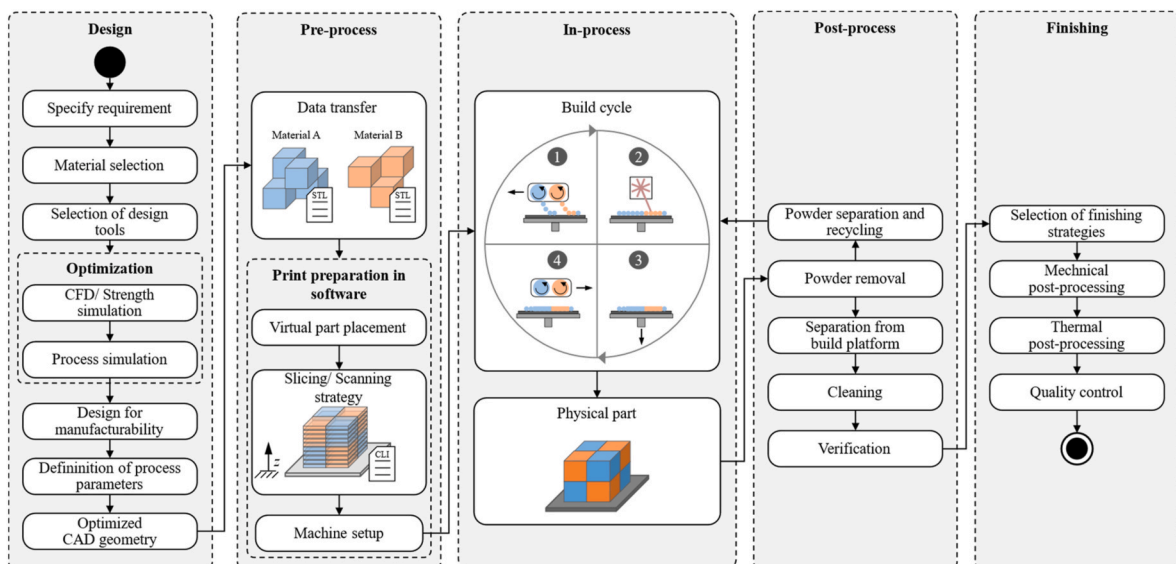


Fig. 2. PBF-LB process chain for multi-material manufacturing.

Suitable design tools must be selected for the geometric modeling of multi-material parts. Since the tools for multi-material manufacturing are currently insufficient, classic CAD programs such as Autodesk Inventor or SOLIDWORKS are usually still used. This involves creating a separate 3D volume model for each material domain in order to subsequently assign suitable process parameters [26,27]. Therefore, new approaches are necessary for the realization of a requirement-specific material allocation at the desired areas. Altenhofen et al. [26] present a novel modeling method, which is particularly suitable for the generation of graded material transitions in volumetric models. This is done by generating NURBS (Non-Uniform Rational B-Splines) volumes based on an isogeometric analysis (IGA). This approach has been implemented by the Fraunhofer IGD as part of the software GramMaCAD (Graded Multi-Material CAD), which enables the user to assign locally varying material properties within a 3D model [36]. Two other tools, GrabCAD Print and Autodesk Monolith, are also worth mentioning in the context of material assignment in volumetric models.

Before determining the process parameters and scanning strategies for individual materials prior to the build cycle, the material compatibility must be verified with respect to the melt pool behavior of the interface morphology. It is well known that defects such as cracks and pores can occur in the joining zone due to various thermal-physical properties such as laser absorptivity and thermal conductivity [21,37,38]. In order to prevent or minimize these effects, two different measures can be taken [28]. One is the optimization of the process parameters [21,39,40] and the other is the determination of suitable geometries along the interfaces [28, 41–44]. The objective is to produce the highest possible relative density and a defect-free material in order to achieve sufficient part quality. At present, qualification of materials for the PBF-LB process is typically performed through a large number of experimental trials, which involve a long lead time and high cost [21,28]. Thus, in order to minimize the effort, current research studies mainly consider a single laser track. This allows relevant parameters such as laser power and scanning speed to be identified. However, in order to optimize scanning strategies or to be able to make statements about pores in the microstructure, investigations of three-dimensional part geometries are essential. A further approach is the use of numerical analyses, which can predict the underlying physical behavior during the PBF-LB manufacturing process for multi-material production [45]. At present, multi-material simulation is not possible using commercially available software. Therefore, a number of research groups have been working on building simulation models to analyze such parts [46]. A major challenge in this regard is the discrepancy between the sizing and time dimensions. Simulating the entire part leads to disproportionately high computational costs given the high temporal and spatial resolution required to investigate the melting process [47]. In consequence, a step-by-step workflow using a multiscale approach is often followed. Initially, a single laser trace is examined, which allows properties such as heat input, thermal emission, phase transition, and surface tension to be investigated [41,48]. This allows the melt pool geometry to be determined, which is then used as input parameters for the heat source of the single-layer model. Lastly, the thermal and mechanical influences on the part level can be calculated which allows conclusions about potential process-induced part warpage to be drawn [46,49,50]. Although additive manufacturing offers a high degree of design freedom compared to conventional manufacturing processes, material-, process- and machine-specific restrictions and rules have to be taken into account during the design process. Currently, no manufacturing restrictions and design guidelines are available for multi-material manufacturing [3,9,24]. In contrast, a large number of PBF-LB design guidelines are known for mono-materials [51]. For example, Kumke et al. [52] provide a comprehensive list of design guidelines. Furthermore, it is currently common practice in data preparation to create a separate sub-solid model for each varying material as well as process parameter, which are then exported to three-dimensional STL (Standard Triangulation Format) facet model files. Other available file formats such as AMF (Additive Manufacturing File Format) or 3MF (3D Manufacturing Format) can, in contrast to STL, contain additional information on the material, surface and other physical properties, but are currently not widely adopted by machine manufacturers [9, 52–54].

2.2.2. Pre-process & in-process

Before parts can be manufactured during in-process, they must first be prepared for machine setup during pre-process. This involves creating layer files from the STL sub-models using a preparation toolset such as Autodesk Netfabb or Materialise Magics. The individual process steps involved are as follows:

1. Virtual placement of the parts onto the particular machine build platform
2. Slicing according to the desired layer thickness
3. Selection of the hatch filling pattern (Simple, Stripe, Quad, Checkerboard)
4. Generation of filling for each parameter set (hatch distance, pattern width, angle allocation)
5. Export of contours and hatching as CLI (Common Layer Interface) files.

This preparation process is associated with high time and effort labor [9,24,28]. Moreover, it involves exporting large amounts of data. Therefore, more efficient part preparation tools, e.g. material-specific build processors, with a higher degree of automation will be necessary in the future.

The virtual part data from the pre-process is then fed to the additive multi-material machine, allowing the physical part to be generated layer-by-layer in the in-process. Most research has investigated 2D multi-material specimens, as these can be manufactured with commercially available PBF-LB machines by means of a manual material change in the z-direction [14,37,55]. In contrast, when manufacturing 3D multi-material parts, spatial control over material distribution is essential [56]. Common recoating mechanisms do not enable a multi-material deposition in the x-y plane [19]. Consequently, one of the current core research topics is the development of apparatuses for multi-material deposition [14].

Fig. 2 illustrates a schematic build cycle that enables a three-dimensional material distribution at the voxel level. This deposition principle uses a separate drum for each material powder [57]. The drums are equipped with a fine-mesh surface, enabling powder

particles to adhere to the drums by means of a vacuum generated via a controlled gas flow. They particles are then selectively deposited during the application of each layer [15]. The build cycle is fully automatic and consists of the following iterative steps:

1. Two-dimensional powder deposition of material A and B
2. Selective melting and solidification of the powder bed
3. Lowering of the build platform by a predefined layer thickness
4. Movement of the recoater to the initial position and repetition of step 1 for layer $n+1$.

Using in-situ process monitoring, it is possible to generate data during the build cycle that provides detailed information about the melting procedure, allowing the underlying causes of part defects to be identified at an early stage and corrected if necessary. With respect to the PBF-LB process, McCann et al. provide a current overview of in-situ process monitoring principles [58]. Particularly noteworthy in this regard are the pyrometer, which can detect overheating or undercooling of the melt pool, and the high-speed camera, which enables visual assessment of the melt pool. At present, so-called open-loop systems are typically used in current implementations of process monitoring, in which the parameters are not adjusted until after analysis in post-processing. By contrast, the novel closed-loop approach allows automated parameter adjustments in real time [59]. Furthermore, machine learning can be used as a means for automated evaluation and classification of sensor data. However, the research status for doing so is still in the developing stage [58,60]. Further literature in this research area can be found in the contributions of [59,61–64].

2.2.3. Post-processing & finishing

In post-processing of the finished part, the fundamental steps and challenges, such as powder removal, part separation from the build platform, evaluation of in-situ process monitoring, post-processing and quality control, are identical for mono- and multi-materials. Currently, however, there are no specific guidelines for mechanical and thermal post-processing of multi-material parts [24].

The clean separation of mixed powders represents an additional process step. This step involves both the separation of the various powder materials from each other as well as the removal of process-related impurities (classifying). Since the particle sizes involved in voxel-wise material deposition are similar, the current state of the art for material separation is proving to be challenging and has not yet been implemented in practice [9,17,28]. There is a need to investigate novel approaches that exploit the physical material properties - such as magnetizability, density, electrical conductivity, surface wettability and chemical or mechanical properties [28]. In the selection of a suitable separation principle, the properties of the materials that exhibit the greatest possible differences should be taken into account [65]. Of significant relevance for this area are the works of the Fraunhofer IGCV, which, in addition to the technical trial and implementation of relevant sorting procedures, also consider methodologies for their selection and evaluation [9,66–68]. In addition to the technical feasibility, the economic viability of the entire powder process chain is considered, in order to be able to select the optimal sorting process for a particular application. In this context, ferromagnetic separation and sieving are particularly worthy of mention, as they have proven to be the most promising processes [66].

When validating the part, it is useful to conduct investigations concerning mechanical and thermal parameters as well as microstructural analyses in the joining zone. In this regard, there have been several investigations in research related to the characterization of the joining zone of 2D specimens using optical methods such as optical- and scanning electron microscope (SEM) images to analyze the microstructure and make statements about the strength and defects [13,19,21–23,37,55,69,70].

3. Materials and methods

In the following, the approach and initial conditions for the determination of PBF-LB/MM design guidelines for the material combination CuCrZr/316L are presented. On the basis of the studies by Adam et al. Wegner and Witt et al. Thomas et al. and Schäfer et al. which employ a systematic approach for the development of design rules, the four steps “consultation of experts/machine manufacturers”, “development of test specimens and selection of suitable measuring equipment”, “production of test specimens with varying characteristics” and “quality inspection and evaluation” can be identified, which were also used in the context of this work [71–74].

Fundamentally, the overall quality of multi-material test specimens produced by PBF-LB is dependent on a large number of influencing parameters. Table 1 provides an overview of the main influencing parameters. This paper differentiates between largely non-influenceable boundary conditions, such as machine, process and powder specifications, and influenceable parameters, such as geometry and scanning specifications.

Table 1
Essential influencing variables for the production of PBF-LB test specimens.

Machine specification	Process specification	Powder specification	Geometry specification	Scan specification
Spot size	Scanning system	Morphology	Discrete/graded	Laser power
Powder delivery system	Monitoring	Particle size	2D/3D	Scan speed
Build Space	Inert gas atmosphere	Condition	Shape	Hatch distance
			Dimension	

3.1. Machine and process specification

To implement the multi-material design, an Aconity MIDI + machine is used with an integrated Aerosint SPD Recoater V1.0. Table 2 lists the key data for the machine and process specifications.

3.2. Powder specification

Fig. 3a and b shows the chemical compositions and the corresponding cumulative particle size distributions specified by the manufacturer of the 316L (Carpenter Additive) and CuCrZr (Eckart TLS GmbH) powders used. The particle size distribution has a crucial influence on powder flowability and the density of the powder bed. When determining the largest particles in a powder size distribution, the percentile value of d_{90} is a key variable. The particle size d_{90} was found to be 24 μm for 316L and 27 μm for CuCrZr, which means that 90% of the particles are smaller than 24 μm and 27 μm , respectively. The particle size distribution requirement for the employed PBF-LB system ranges from 15 to 35 μm . These non-customary sizing requirements are necessary to ensure adhesion to the drums for powder deposition. Furthermore, the particle shape of the powder was examined using an optical microscope. A spherical morphology of the particles was observed, which is required in order to achieve a powder bed that is as dense and homogeneous as possible (see Fig. 3c).

3.3. Geometry specification

For the fundamental evaluation of the PBF-LB/MM system, this paper primarily considers five different characteristic features. The test specimens are listed along with their varied parameter ranges in Table 3. To evaluate the manufacturability of part clearances and downskin angles, pre-existing mono-material test specimens according to DIN 52902 are used (see Table 3a and b) [DIN52902]. For the multi-material test specimens, the anisotropy of the material variation, the voxel size within a gradation and the scanning parameters are investigated. For this purpose, different interfacial geometries are considered. The most basic method to join materials together is the butt joint (see feature: anisotropy, Table 3c). The joint geometry with an interlocking contour follows the approach of increasing the size of the contact area (see feature: laser power, Table 3e). The graded material transition can be regarded as a connection geometry in which stress concentrations and the associated defects are to be prevented by creating an enlarged transition zone (see feature: grading, Table 3d). In addition to the specimens for which features were assigned, control specimens were generated that are initially exposed in a build cycle in order to verify the laser alignment, i.e. the correspondence between the deposition and scan contours, in advance and to be able to adjust the PBF-LB/MM system if necessary (see control specimens, Table 3f). Furthermore, it is important to note that all specimens were manufactured without support structures and no post heat treatment was performed.

3.4. Scan specification

The initial data for the scan parameters are given in Table 4a (manufacturer specifications of Aerosint). In this work, the volume energy density is considered as a comparison value. This value describes the amount of energy that the laser beam introduces into the material per volumetric unit and is calculated from the quotient of the laser power and the product of the scan speed, layer thickness and hatch distance. The interaction between the laser beam and the absorption characteristics of the material has a significant influence on the resulting part quality. Since the copper alloy has a high thermal conductivity and lower absorption rate of the laser energy at a wavelength range of 1070 nm compared to the steel alloy, it requires a higher volumetric energy density to melt the material. Additionally, the powder layer of the copper alloy is melted a second time at a 90° angle offset from the previous layer. This is also referred to as remelting and results in lower crack formation, porosity and reduced residual stress while simultaneously increasing the part density. Furthermore, a stripe pattern is used for hatch filling, in which the minimum track width is limited to 0.08 mm by the laser spot diameter. For the evaluation of the scan data, the laser power and scanning speed were varied according to Table 4b.

Table 2
Machine and process data.

Machine	Aconity MIDI+ with integrated Aerosint SPD Recoater V1.0	Spot size	80 μm
Software	AconitySTUDIO	Laser	500 W and 1000 W
		Build surface (x-y)	96 x 220 mm^2
		Recoating speed	10 mm/s
		Powder pixel resolution	500 μm
		Inline process view	Camera
		Inert gas	Argon 4.8

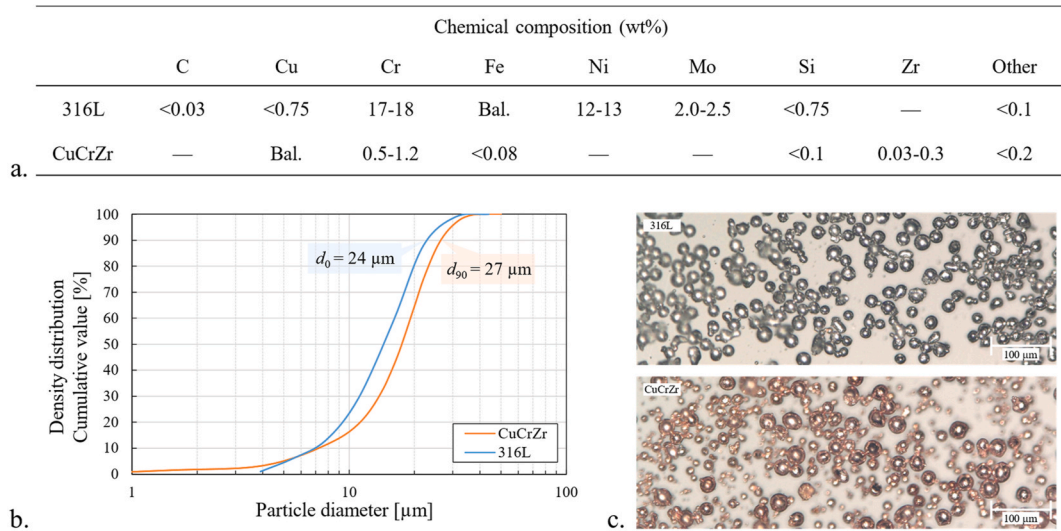
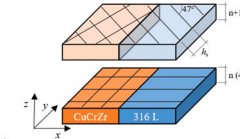


Fig. 3. Powder material, a. Chemical composition of the materials used, b. Logarithmic particle size distribution, c. Spherical morphology using the example of 316L

Table 3
Characteristic features and test specimens.

<p>a)</p> <p>Feature Category: Length x Width, Height, Slot width</p> <p>Part spacing Arrangement: 28,4 x 17,1 mm², 5 mm, 1,0/0,8/0,6/0,4/0,2/0,1 mm</p>	<p>b)</p> <p>Feature Category: Length x Width, Height, Flat tabs dimensions, Downskin angle</p> <p>Downskin angle: 0°/15°/30°/45°/60°/75°/90°</p>
<p>c)</p> <p>Feature Category: Length x Width, Height, Build direction of the materials</p> <p>Anisotropy Arrangement: 10 x 10 mm², 10 mm, 316L→CuCrZr/ CuCrZr→316L/ CuCrZr→316L</p>	<p>d)</p> <p>Feature Category: Length x Width, Height, Voxel size</p> <p>Grading Size: 60 x 15,4 mm², 6 mm, 0,2/0,5/1/2 mm</p>
<p>e)</p> <p>Feature Category: Length x Width, Height, Volumetric Energy Density CuCrZr</p> <p>Laser power Laser scanning: 10 x 10 mm², 5 mm, 69/104/139/174/208 J/mm³</p>	<p>f)</p> <p>Control specimens (exemplary) Purpose: Verify the laser alignment</p>

Table 4
Scanning parameters, a. Boundary conditions, b. Parameter set with constant scan speed of 600 mm/s.



	Laser power P_L [W]	Scan speed v_s [mm/s]	Hatch distance h_s [mm]	Laser power P_L [W]	Volumetric Energy Density E_v [J/mm ³]
316L	150	600	0.08	200	69.40
CuCrZr	500	550	0.12	300	104.2
CuCrZr	500	600	0.12	400	138.9
CuCrZr (Re-melting)	500	600	0.12	500	173.6
				600	208.3

3.5. Measurement procedure

This work primarily uses optical inspection procedures, such as visual inspection and a scanning electron microscope (SEM), as well as radiographic inspection using micro-computed tomography (μ CT). The in-process is recorded using a CMOS camera, which allows defects to be detected during the build cycle and corrected if necessary. Fig. 4a shows a photo taken after a recoating cycle and Fig. 4b links to a video recording of the scanning process.

After the build cycle, the first step is to evaluate the manufacturability of the test specimens by means of visual inspection at a macroscopic level. In the next step, selected test specimens are examined in detail using additional equipment that provides a view into the interior of the specimen at a microscopic level. The SEM can be used for microstructural examination, in particular for the detection of defects in the joining zone of different materials. μ CT, on the other hand, allows defects in the entire three-dimensional test specimen to be examined and analyzed in any sectional plane. This enables even complicated geometries of test specimens to be inspected for dimensional accuracy as well as surface roughness.

4. Results and discussion

The results obtained from the considered characteristic features from Table 3 are presented in Table 5. For the assessment of manufacturability, Harvey balls indicating “successfully manufacturable” (black filled circle) and “not manufacturable” (white filled circle) are used.

4.1. Part spacing and downskin angle

Table 5a and b shows the different features “slot width” and “downskin angle” for the mono-material specimens of the materials 316L and CuCrZr. All test specimens could be manufactured in their entirety. Thus, it can be generally confirmed that the given machine, process and powder specifications lead to the desired results. In order to determine the smallest achievable distance between two slots or parts, the slot width is measured with the aid of a feeler gauge in the measurement range from 0.05 to 1 mm and compared with the nominal values [75]. It was found that the actual values were on average 0.3 mm smaller than the nominal values. Gaps below 0.6 mm cannot be manufactured. From these results, it can be concluded that a minimum spacing of 1 mm can be successfully manufactured. The investigation of downskin angles showed that all flat tabs (length 15 mm) could be fabricated with angles from 15° to 90°. However, significant differences can be seen both between the tabs themselves and between their corresponding downskin and upskin surfaces (see Table 5b). A self-supporting downskin angle of 30° is recommended in this case. It is important to mention in this context that the investigation presented here is based on random samples and that further research will be required for statistically validated measurements in the future.

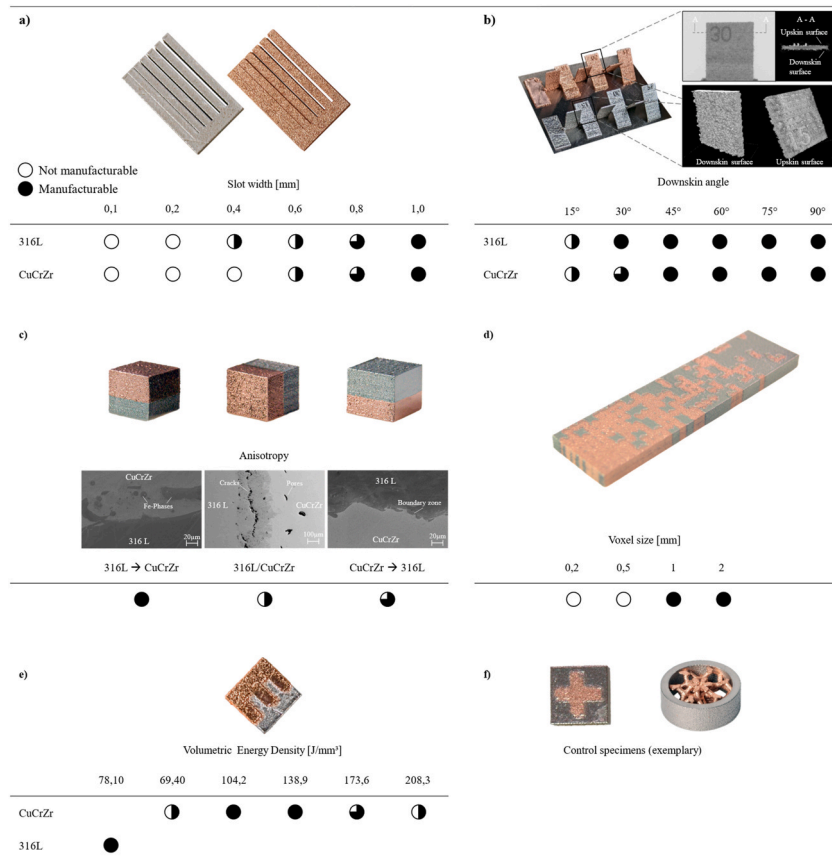
4.2. Anisotropy

To investigate the influence of direction-dependent material arrangement on part quality, SEM images were acquired of the manufactured cubical test specimens (see Table 5c). In each specimen, the inner core of the polished joining zone is examined. The investigations reveal that multi-material manufacturing is a highly anisotropic process and that the build direction of the part has a significant influence on the joining zone. While mixing occurs in the joining zone (interfacial diffusion) in the case of a steel to copper printing sequence, resulting in improved bond strength, no mixing occurs in the case of an inverted arrangement. If both materials lie



Fig. 4. In-situ camera for process monitoring, a. Photo after recoating, b. Video of scanning process.

Table 5
Evaluation of the manufacturability of geometry characteristics.



parallel to the build direction, the joining zone exhibits significant pores and cracks. The findings thus confirm that excessively high temperature gradients during the solidification process lead to defects in the joining zone.

4.3. Grading

Two out of the four graded samples could be manufactured. Due to the large number of voxels, transferring the part data to the multi-material machine proved to be a challenging task. The smallest achievable voxel size is 1 mm. A completely continuous material transition cannot be produced in the joining zone. The individual voxels of the materials are discretely separated from each other.

4.4. Laser power

The scan parameters of CuCrZr are investigated on a geometry-specific basis using 3D-specimens. Compared to the butt joint, the interlocked joint contour has a 62% larger surface area of contact. The results show that all the parameters varied are within the feasible process window in the range from 78 to 208 J/mm³, though significant differences can still be observed between them. The recommended laser power for CuCrZr in this case is 400 W or a volume energy density of 139 J/mm³, which results in a more homogeneous melt pool in the joining zone with 316L compared to the initial parameters (500 W).

4.5. Design guidelines

In addition to the five characteristics previously studied, new machine- and process-specific findings could also be obtained by means of process monitoring. All results were formalized in material- and process-specific design guidelines in the form of a catalog (see Figs. 5 and 6). A total of twelve guidelines could be identified, which, for the sake of clarity, are classified into six characteristic groups: arrangement, size, overhangs, economy, powder quality, laser exposure. This includes representative examples, a description and, where appropriate, specific values.

Structure		Unfavorable	Favorable	Explanation		
1	Part/material-specific	Arrangement	Recoater		Reduce recoater forces on the part. Minimize the contact area with the recoater.	
			Anisotropy		Avoid pores and cracks whenever possible. The materials in the part should be oriented according to a homogeneous melt pool.	
			Part spacing		Insufficient spacing results in thermal interaction between parts. The smallest achievable distance between two parts or slots is $a_{316L} = a_{CuCr1Zr} = 1 \text{ mm}$. (Resolution slot according to DIN 52902)	
			Overhangs	Downskin		The self-supporting downskin angle is approx. $\delta_{316L} = \delta_{CuCr1Zr} = 30^\circ$. (Test specimen according to DIN 52902; 40 μm layer thickness; length 15 mm)
			Size	Grading		The smallest voxel size for a material grading is about 1 mm.
			Economy	Deposition		To save costs, the powder bed is coated with the less expensive feedstock as filler material.

Fig. 5. Part/material-specific design guidelines.

5. Summary and outlook

Compared to the additive manufacturing of mono-materials, the design solution space can be expanded by using functionally optimized multi-materials. For reaching industrial maturity, design guidelines are necessary to act as supporting tools during the design phase. The aim of this work is to develop process-specific PBF-LB/MM design guidelines for the 316L/CuCrZr material combination. Selected characteristic features were investigated, differing in geometry and scan specifications. With the boundary conditions considered in this work, it was possible to fabricate specimens with arbitrarily placed materials within a build plane. Entirely novel machine- and process-specific insights could be gained compared to mono-material manufacturing. For example, the inert gas flow should be switched off during powder deposition in order to avoid powder contamination. Currently, the phenomena of crack and pore formation in the joining zone due to differences in material properties pose a major challenge in PBF-LB/MM manufacturing. This particular effect was also identified in this paper, specifically in the case of a flat butt joint with a material transition in the build plane.

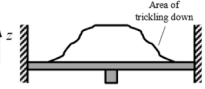
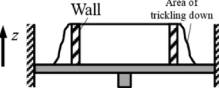
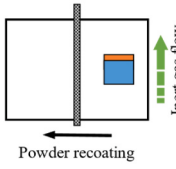
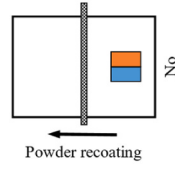
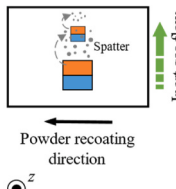
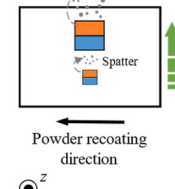
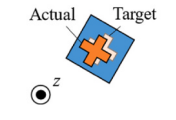

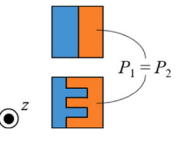
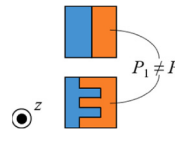
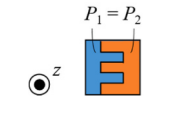
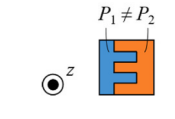
Structure		Unfavorable	Favorable	Explanation
7 8 9 10 11 12	Powder bed quality	Wall 	Wall 	Prevent powder from trickling down from the powder heap, since it is not supported by the build platform cylinder. Incorporate a boundary wall from a height of approx. 5 mm.
		Deposition 	Deposition 	Avoid powder contamination caused by the inert gas flow. Do not use inert gas during powder deposition.
	Laser scanning	Order 	Order 	Place parts with larger cross sections to conform to the inert gas flow in order to minimize spatter contamination. Adjust the scan sequence accordingly.
		Alignment 	Alignment 	Verify alignment of deposited material and laser contour. Use control specimens.
		Power (geometry) 	Power (geometry) 	The laser power must be adjusted depending on the geometry.
		Power (material) 	Power (material) 	The laser power must be adjusted to suit the material. (Recommended parameters: $P_L = 150\text{ W}$; $v_s = 600\text{ mm/s}$ for 316L and $P_L = 400\text{ W}$; $v_s = 600\text{ mm/s}$ for CuCrZr; $D_s = 40\text{ }\mu\text{m}$)

Fig. 6. Machine/process-specific design guidelines.

By contrast, no defects were observed in the case of a material transition from steel to copper in the build direction. Here, material mixing takes place in the joining zone, which results in an improved bond strength. Multi-material manufacturing is therefore a strongly anisotropic process where the material arrangement has a significant influence on the joining zone.

The investigations show that it is possible to manufacture different interface geometries, such as a rectangular interlocking geometry or a graded material transition, using this process-specific PBF-LB/MM method. However, no completely continuous material transition can be realized using the graded material transition. The smallest achievable particle size for material grading is approximately 1 mm. Furthermore, suitable process parameters were identified using three-dimensional test specimens for CuCrZr in order to

achieve a homogeneous melt pool and a defect-free joining zone. For CuCrZr, a process window for the volumetric energy density in the range of 104–174 J/mm³ is recommended. The process parameters must be adjusted both material-specific and, in particular, geometry-specific.

Future work is needed to investigate this effect in more detail in order to gain further control over component quality. There are several possible measures to achieve this. On the one hand, further optimization of the interface geometry is needed, on the other hand, the partial variation of the process parameters along the joining zone needs to be investigated. Furthermore, post-process heat treatment strategies, such as hot isostatic pressing (HIP) for redensification of the test specimens, could be investigated. In order to obtain more detailed information about the melt pool behavior during the build cycle, additional tools such as pyrometers and high-speed cameras should be used in future research work. The findings established in this paper provide an initial foundation for comprehensive PBF-LB/MM design guidelines and can be expanded in further research for arbitrary materials, geometry features, as well as processes.

Author contribution statement

Ina Meyer: Conceived and designed the experiments; Performed the experiments; Analyzed and interpreted the data; Contributed reagents, materials, analysis tools or data; Wrote the paper. Marcus Oel: Performed the experiments. Tobias Ehlers: Conceived and designed the experiments; Wrote the paper. Roland Lachmayer: Conceived and designed the experiments.

Data availability statement

Data will be made available on request.

Declaration of competing interest

The authors declare that they have no known competing financial interests or personal relationships that could have appeared to influence the work reported in this paper.

Acknowledgment

This research has been funded by the Ministry for Science and Culture of Lower Saxony (MWK) – School for Additive Manufacturing SAM.

The project “Major Research Instrumentation for integration of efficient effects in multi-material structural components” was funded by the Deutsche Forschungsgemeinschaft (DFG, German Research Foundation) - Project number 445707542.

The project “Computer tomograph for optomechatronic systems” was funded by the Deutsche Forschungsgemeinschaft (DFG, German Research Foundation) - Project number 432176896.

References

- [1] R. Lachmayer, T. Ehlers, R.B. Lippert, *Entwicklungsmethodik für die Additive Fertigung*, second ed., Springer Berlin Heidelberg, Berlin, Heidelberg, 2022 <https://doi.org/10.1007/978-3-662-65924-3>.
- [2] M. Binder, C. Dirnhofer, P. Kindermann, M. Horn, M. Schmitt, C. Anstaett, G. Schlick, C. Seidel, G. Reinhart, Procedure and validation of the implementation of automated sensor integration kinematics in an LPBF system, *Procedia CIRP* 93 (2020) 1304–1309, <https://doi.org/10.1016/j.procir.2020.04.090>.
- [3] A. Reichardt, A.A. Shapiro, R. Otis, R.P. Dillon, J.P. Borgonia, B.W. McEnerney, P. Hosemann, A.M. Beese, Advances in additive manufacturing of metal-based functionally graded materials, *Int. Mater. Rev.* 66 (2021) 1–29, <https://doi.org/10.1080/09506608.2019.1709354>.
- [4] T.T. Wohlers, R.I. Campbell, O. Diegel, J. Kowen, R. Huff, N. Mostow, I. Fidan, D.L. Bourell, J. Van Rensburg, *Wohlers Report 2022: 3D Printing and Additive Manufacturing Global State of the Industry*, Wohlers Associates, 2022.
- [5] R. Lachmayer, B.A. Behrens, T. Ehlers, P. Müller, P. Althaus, M. Oel, E. Farahmand, P.C. Gembariski, H. Wester, S. Hübner, Process-integrated lubrication in sheet metal forming, *Journal of Manufacturing and Materials Processing* 6 (2022), <https://doi.org/10.3390/jmmp6050121>.
- [6] L. Meng, W. Zhang, D. Quan, G. Shi, L. Tang, Y. Hou, P. Breikopf, J. Zhu, T. Gao, From topology optimization design to additive manufacturing: today's success and tomorrow's roadmap, *Arch. Comput. Methods Eng.* 27 (2020) 805–830, <https://doi.org/10.1007/s11831-019-09331-1>.
- [7] C. Wei, Z. Zhang, D. Cheng, Z. Sun, M. Zhu, L. Li, An overview of laser-based multiple metallic material additive manufacturing: from macro: from micro-scales, *Int. J. Extrem. Manuf.* 3 (2021), <https://doi.org/10.1088/2631-7990/abce04>.
- [8] Y. Kok, X.P. Tan, P. Wang, M.L.S. Nai, N.H. Loh, E. Liu, S.B. Tor, Anisotropy and heterogeneity of microstructure and mechanical properties in metal additive manufacturing: a critical review, *Mater. Des.* 139 (2018) 565–586, <https://doi.org/10.1016/j.matdes.2017.11.021>.
- [9] M. Binder, C. Anstaett, M. Horn, F. Herzer, G. Schlick, C. Seidel, J. Schilp, G. Reinhart, Potentials and challenges of multi-material processing by laser-based powder bed fusion, *Solid Freeform Fabrication*, in: 2018: Proceedings of the 29th Annual International Solid Freeform Fabrication Symposium - an Additive Manufacturing Conference, SFF 2018, 2018, pp. 376–387, <https://doi.org/10.26153/tsw/17025>.
- [10] T. Ehlers, R. Lachmayer, Design of particle dampers for laser powder bed fusion, *Appl. Sci.* 12 (2022), <https://doi.org/10.3390/app12042237>.
- [11] e.V. VDI Verein Deutscher Ingenieure, *Additive Fertigung Additive Manufacturing 3-D-Druckverfahren sind Realität in der industriellen Fertigung - VDI-Statusreport November 2019*, 2019, <https://www.vdi.de/ueber-uns/presse/publikationen/details/3-d-druckverfahren-sind-realitaet-in-der-industriellen-fertigung>, accessed December 12, 2022.
- [12] T. Ehlers, I. Meyer, M. Oel, B. Bode, P.C. Gembariski, R. Lachmayer, Effect-Engineering by Additive Manufacturing, *Innovative Product Development by Additive Manufacturing* 2021, 2023, pp. 1–19, https://doi.org/10.1007/978-3-031-05918-6_1.
- [13] C. Anstaett, C. Seidel, G. Reinhart, Fabrication of 3D multi-material parts using laser-based powder bed fusion, in: *International Solid Freeform Fabrication Symposium*, 2017, <https://hdl.handle.net/2152/89963>, accessed December 12, 2022.
- [14] B. Neirincx, X. Li, M. Hick, Powder deposition systems used in powder bed-based multimetal additive manufacturing, *Acc Mater Res* 2 (2021) 387–393, <https://doi.org/10.1021/accountsmr.1c00030>.

- [15] Kevin Eckes, How to Make Cheap, Scalable Multi Material 3D Printing a Reality, Aerosint SA, 2018. <https://aerosint.com/how-to-make-cheap-scalable-multi-material-3d-printing-a-reality/>. accessed December 12, 2022.
- [16] D. Gu, X. Shi, R. Poprawe, D.L. Bourell, R. Setchi, J. Zhu, Material-structure-performance integrated laser-metal additive manufacturing, *Science* (2021) 372, <https://doi.org/10.1126/science.abg1487>.
- [17] C. Wei, L. Li, Recent progress and scientific challenges in multi-material additive manufacturing via laser-based powder bed fusion, *Virtual Phys. Prototyp.* 16 (2021) 347–371, <https://doi.org/10.1080/17452759.2021.1928520>.
- [18] K.J. Jakubenas, J.M. Sanchez, H.L. Marcus, Multiple material solid free-form fabrication by selective area laser deposition, *Mater. Des.* 19 (1998) 11–18, [https://doi.org/10.1016/S0261-3069\(98\)00004-1](https://doi.org/10.1016/S0261-3069(98)00004-1).
- [19] C. Wei, Z. Sun, Q. Chen, Z. Liu, L. Li, Additive manufacturing of horizontal and 3D functionally graded 316L/Cu10Sn components via multiple material selective laser melting, *J. Manuf. Sci. Eng.* 141 (2019) 1–8, <https://doi.org/10.1115/1.4043983>.
- [20] M. Vaezi, S. Chianrabutra, B. Mellor, S. Yang, Multiple material additive manufacturing – Part 1: a review, *Virtual Phys. Prototyp.* 8 (2013) 19–50, <https://doi.org/10.1080/17452759.2013.778175>.
- [21] J. Chen, Y. Yang, C. Song, D. Wang, S. Wu, M. Zhang, Influence mechanism of process parameters on the interfacial characterization of selective laser melting 316L/CuSn10, *Mater. Sci. Eng.* 792 (2020), 139316, <https://doi.org/10.1016/j.msea.2020.139316>.
- [22] C. Tan, Y. Chew, G. Bi, D. Wang, W. Ma, Y. Yang, K. Zhou, Additive manufacturing of steel–copper functionally graded material with ultrahigh bonding strength, *J. Mater. Sci. Technol.* 72 (2021) 217–222, <https://doi.org/10.1016/j.jmst.2020.07.044>.
- [23] S. Mao, D.Z. Zhang, Z. Ren, G. Fu, X. Ma, Effects of process parameters on interfacial characterization and mechanical properties of 316L/CuCrZr functionally graded material by selective laser melting, *J. Alloys Compd.* 899 (2022), 163256, <https://doi.org/10.1016/j.jallcom.2021.163256>.
- [24] M. Schneck, M. Horn, M. Schmitt, C. Seidel, G. Schlick, G. Reinhart, Review on additive hybrid- and multi-material-manufacturing of metals by powder bed fusion: state of technology and development potential, *Progress in Additive Manufacturing* 6 (2021) 881–894, <https://doi.org/10.1007/s40964-021-00205-2>.
- [25] S.L. Sing, S. Huang, G.D. Goh, G.L. Goh, C.F. Tey, J.H.K. Tan, W.Y. Yeong, Emerging metallic systems for additive manufacturing: in-situ alloying and multi-metal processing in laser powder bed fusion, *Prog. Mater. Sci.* 119 (2021), 100795, <https://doi.org/10.1016/j.pmatsci.2021.100795>.
- [26] C. Altenhofen, T.H. Luu, T. Grasser, M. Dennstädt, J.S. Mueller-Roemer, D. Weber, A. Stork, Continuous property gradation for multi-material 3D-printed objects, in: *Solid Freeform Fabrication 2018: Proceedings of the 29th Annual International Solid Freeform Fabrication Symposium - An Additive Manufacturing Conference*, 2018, pp. 1675–1685, <https://doi.org/10.26153/tsw/17159>.
- [27] X. Yao, S.K. Moon, G. Bi, J. Wei, A multi-material part design framework in additive manufacturing, *Int. J. Adv. Manuf. Technol.* 99 (2018) 2111–2119, <https://doi.org/10.1007/s00170-018-2025-7>.
- [28] D. Wang, L. Liu, G. Deng, C. Deng, Y. Bai, Y. Yang, W. Wu, J. Chen, Y. Liu, Y. Wang, X. Lin, C. Han, Recent progress on additive manufacturing of multi-material structures with laser powder bed fusion, *Virtual Phys. Prototyp.* 17 (2022) 329–365, <https://doi.org/10.1080/17452759.2022.2028343>.
- [29] Deutsches Institut für Normung e. V., DIN EN ISO/ASTM 52902:2020-05 - Additive Fertigung - Testkörper - Allgemeine Leitlinie für die Bewertung der geometrischen Leistung additiver Fertigungssysteme (AM-Systeme) (ISO/ASTM 52902:2019), Beuth Verlag GmbH, Berlin, 2020.
- [30] C. Anstaett, C. Seidel, G. Reinhart, Herstellung von 3-D-Multimaterialbauteilen aus Kupfer-Chrom-Zirkonium und Werkzeugstahl 1.2709, in: *Rapid.Tech + FabCon 3.D – International Trade Show + Conference for Additive Manufacturing*, Carl Hanser Verlag GmbH & Co. KG, München, 2018, pp. 330–344, <https://doi.org/10.3139/9783446458123.021>.
- [31] M. Ott, Multimaterialverarbeitung bei der additiven strahl- und pulverbettbasierten Fertigung, Dissertation, Technische Universität München, 2012. <https://nbn-resolving.de/urn:nbn:de:bvb:91-diss-20120703-1095129-1-6>.
- [32] S. Girnth, J. Koopmann, G. Klawitter, N. Waldt, T. Niendorf, 3D hybrid-material processing in selective laser melting: implementation of a selective coating system, *Progress in Additive Manufacturing* 4 (2019) 399–409, <https://doi.org/10.1007/s40964-019-00082-w>.
- [33] M.F. Ashby, Y.J.M. Bréchet, D. Cebon, L. Salvo, Selection strategies for materials and processes, *Mater. Des.* 25 (2004) 51–67, [https://doi.org/10.1016/S0261-3069\(03\)00159-6](https://doi.org/10.1016/S0261-3069(03)00159-6).
- [34] T. Brockmüller, I. Mozgova, R. Lachmayer, An approach to analyse the potential of tailored forming by TRIZ Reverse, in: *DS 87-4 Proceedings of the 21st International Conference on Engineering Design (ICED 17) Vol 4, Design Methods and Tools*, Vancouver, Canada, 2017, pp. 445–452.
- [35] Z. Chen, C. Han, M. Gao, S.Y. Kandukuri, K. Zhou, A review on qualification and certification for metal additive manufacturing, *Virtual Phys. Prototyp.* 17 (2022) 382–405, <https://doi.org/10.1080/17452759.2021.2018938>.
- [36] D. Welling, CAD-Modelle gradieren – elegant, funktional und intuitiv, Fraunhofer-Institut Für Graphische Datenverarbeitung (IGD) - Presseinformation, 2021. <https://www.igd.fraunhofer.de/de/media-center/presse/cad-modelle-gradieren—elegant-funktional-und-intuitiv-.html>. accessed December 13, 2022.
- [37] Z.H. Liu, D.Q. Zhang, S.L. Sing, C.K. Chua, L.E. Loh, Interfacial characterization of SLM parts in multi-material processing: metallurgical diffusion between 316L stainless steel and C18400 copper alloy, *Mater. Char.* 94 (2014) 116–125, <https://doi.org/10.1016/j.matchar.2014.05.001>.
- [38] X. Mei, X. Wang, Y. Peng, H. Gu, G. Zhong, S. Yang, Interfacial characterization and mechanical properties of 316L stainless steel/inconel 718 manufactured by selective laser melting, *Mater. Sci. Eng.* 758 (2019) 185–191, <https://doi.org/10.1016/j.msea.2019.05.011>.
- [39] B. Rankouhi, S. Jahani, F.E. Pfefferkorn, D.J. Thoma, Compositional grading of a 316L-Cu multi-material part using machine learning for the determination of selective laser melting process parameters, *Addit. Manuf.* 38 (2021), 101836, <https://doi.org/10.1016/j.addma.2021.101836>.
- [40] Z. Liu, D. Zhao, P. Wang, M. Yan, C. Yang, Z. Chen, J. Lu, Z. Lu, Additive manufacturing of metals: microstructure evolution and multistage control, *J. Mater. Sci. Technol.* 100 (2022) 224–236, <https://doi.org/10.1016/j.jmst.2021.06.011>.
- [41] Z. Sun, Y.H. Chueh, L. Li, Multiphase mesoscopic simulation of multiple and functionally gradient materials laser powder bed fusion additive manufacturing processes, *Addit. Manuf.* 35 (2020), 101448, <https://doi.org/10.1016/j.addma.2020.101448>.
- [42] C.F. Tey, X. Tan, S.L. Sing, W.Y. Yeong, Additive manufacturing of multiple materials by selective laser melting: Ti-alloy to stainless steel via a Cu-alloy interlayer, *Addit. Manuf.* 31 (2020), 100970, <https://doi.org/10.1016/j.addma.2019.100970>.
- [43] C. Wei, L. Li, X. Zhang, Y.-H. Chueh, 3D printing of multiple metallic materials via modified selective laser melting, *CIRP Annals* 67 (2018) 245–248, <https://doi.org/10.1016/j.cirp.2018.04.096>.
- [44] Y.-H. Chueh, C. Wei, X. Zhang, L. Li, Integrated laser-based powder bed fusion and fused filament fabrication for three-dimensional printing of hybrid metal/polymer objects, *Addit. Manuf.* 31 (2020), 100928, <https://doi.org/10.1016/j.addma.2019.100928>.
- [45] L. Yao, S. Huang, U. Ramamurthy, Z. Xiao, On the formation of “Fish-scale” morphology with curved grain interfacial microstructures during selective laser melting of dissimilar alloys, *Acta Mater.* 220 (2021), <https://doi.org/10.1016/j.actamat.2021.117331>.
- [46] H. Gu, C. Wei, L. Li, Q. Han, R. Setchi, M. Ryan, Q. Li, Multi-physics modelling of molten pool development and track formation in multi-track, multi-layer and multi-material selective laser melting, *Int. J. Heat Mass Tran.* 151 (2020), <https://doi.org/10.1016/j.ijheatmasstransfer.2020.119458>.
- [47] M. Käb, M. Werz, S. Weihe, Numerische Simulation zur Vorhersage von Temperaturfeldern, Eigenspannungen und Verzug beim selektiven Laserstrahlschmelzen, in: *Additive Fertigung von Bauteilen Und Strukturen*, Springer Fachmedien Wiesbaden, Wiesbaden, 2019, pp. 199–222, https://doi.org/10.1007/978-3-658-27412-2_13.
- [48] S. Mohanty, J.H. Hattel, Laser additive manufacturing of multimaterial tool inserts: a simulation-based optimization study, *Laser 3D Manufacturing IV 10095* (2017) 100950G, <https://doi.org/10.1117/1.22253600>.
- [49] Z. Chen, Y. Xiang, Z. Wei, P. Wei, B. Lu, L. Zhang, J. Du, Thermal dynamic behavior during selective laser melting of K418 superalloy: numerical simulation and experimental verification, *Appl. Phys. A* 124 (2018) 313, <https://doi.org/10.1007/s00339-018-1737-8>.
- [50] C. Seidel, M.F. Zaeh, Multi-scale modelling approach for contributing to reduced distortion in parts made by laser-based powder bed fusion, *Procedia CIRP* 67 (2018) 197–202, <https://doi.org/10.1016/j.procir.2017.12.199>.
- [51] G.A.O. Adam, D. Zimmer, Design for Additive Manufacturing-Element transitions and aggregated structures, *CIRP J Manuf Sci Technol* 7 (2014) 20–28, <https://doi.org/10.1016/j.cirpj.2013.10.001>.
- [52] M. Kumke, Grundlagen der additiven Fertigung, in: *Methodisches Konstruieren von Additiv Gefertigten Bauteilen*, Springer Fachmedien Wiesbaden, Wiesbaden, 2018, pp. 7–23, https://doi.org/10.1007/978-3-658-22209-3_2.

- [53] A. Gebhardt, Additive Fertigungsverfahren, Carl Hanser Verlag GmbH & Co. KG, München, 2016, <https://doi.org/10.3139/9783446445390>.
- [54] G.H. Loh, E. Pei, D. Harrison, M.D. Monzón, An overview of functionally graded additive manufacturing, *Addit. Manuf.* 23 (2018) 34–44, <https://doi.org/10.1016/j.addma.2018.06.023>.
- [55] S.L. Sing, L.P. Lam, D.Q. Zhang, Z.H. Liu, C.K. Chua, Interfacial characterization of SLM parts in multi-material processing: intermetallic phase formation between AlSi10Mg and C18400 copper alloy, *Mater. Char.* 107 (2015) 220–227, <https://doi.org/10.1016/j.matchar.2015.07.007>.
- [56] T. Stichel, T. Laumer, T. Linnenweber, P. Amend, S. Roth, Mass flow characterization of selective deposition of polymer powders with vibrating nozzles for laser beam melting of multi-material components, *Phys. Procedia* 83 (2016) 947–953, <https://doi.org/10.1016/j.phpro.2016.08.099>.
- [57] M. Rafiee, R.D. Farahani, D. Therriault, Multi-material 3D and 4D printing: a survey, *Adv. Sci.* 7 (2020), 1902307, <https://doi.org/10.1002/adv.201902307>.
- [58] R. McCann, M.A. Obeidi, C. Hughes, É. McCarthy, D.S. Egan, R.K. Vijayaraghavan, A.M. Joshi, V. Acinas Garzon, D.P. Dowling, P.J. McNally, D. Brabazon, In-situ sensing, process monitoring and machine control in Laser Powder Bed Fusion: a review, *Addit. Manuf.* 45 (2021), <https://doi.org/10.1016/j.addma.2021.102058>.
- [59] K. Gutknecht, M. Cloots, R. Sommerhuber, K. Wegener, Mutual comparison of acoustic, pyrometric and thermographic laser powder bed fusion monitoring, *Mater. Des.* 210 (2021), 110036, <https://doi.org/10.1016/j.matdes.2021.110036>.
- [60] P. Yadav, O. Rigo, C. Arvieu, E. le Guen, E. Lacoste, In situ monitoring systems of the SLM process: on the need to develop machine learning models for data processing, *Crystals* 10 (2020) 1–26, <https://doi.org/10.3390/cryst10060524>.
- [61] M. Grasso, A. Remani, A. Dickens, B.M. Colosimo, R.K. Leach, In-situ measurement and monitoring methods for metal powder bed fusion: an updated review, *Meas. Sci. Technol.* 32 (2021), <https://doi.org/10.1088/1361-6501/ac0b6b>.
- [62] T.G. Spears, S.A. Gold, In-process sensing in selective laser melting (SLM) additive manufacturing, *Integr Mater Manuf Innov* 5 (2016) 16–40, <https://doi.org/10.1186/s40192-016-0045-4>.
- [63] B. Wu, X. yuan Ji, J. xin Zhou, H. qing Yang, D. jian Peng, Z. ming Wang, Y. jie Wu, Y. jun Yin, In situ monitoring methods for selective laser melting additive manufacturing process based on images — a review, *China Foundry* 18 (2021) 265–285, <https://doi.org/10.1007/s41230-021-1111-x>.
- [64] Y. Hagedorn, F. Pastors, Process monitoring of laser beam melting, *Laser Technik Journal* 15 (2018) 54–57, <https://doi.org/10.1002/latj.201800009>.
- [65] R. Koller, J. Pielen, Systematik der Prinziplösungen zum Trennen von Stoffen - ein Beitrag zur Konstruktionsmethodik, *Chem. Ing. Tech.* 52 (1980) 695–702, <https://doi.org/10.1002/cite.330520903>.
- [66] C. Seidel, Multi-material metal parts by powder bed fusion: new application opportunities, *Metal AM* 8 (2022) 145–151. <https://www.metal-am.com/articles/multi-material-metal-parts-by-powder-bed-fusion-new-application-opportunities/>. accessed December 12, 2022.
- [67] M. Horn, L. Prestel, M. Schmitt, M. Binder, G. Schlick, C. Seidel, G. Reinhart, Multi-Material additive manufacturing - recycling of binary metal powder mixtures by screening, *Procedia CIRP* 93 (2020) 550–555, <https://doi.org/10.1016/j.procir.2020.04.098>.
- [68] C. Anstätt, Multimaterialverarbeitung mittels Laserstrahlschmelzen am Beispiel von metallischen Verbindungen mit der Kupferlegierung CW106C, Dissertation, Technische Universität München, 2020. <https://nbn-resolving.de/urn/resolver.pl?urn:nbn:de:bvb:91-diss-20200923-1524471-1-1>.
- [69] Y. Bai, J. Zhang, C. Zhao, C. Li, H. Wang, Dual interfacial characterization and property in multi-material selective laser melting of 316L stainless steel and C52400 copper alloy, *Mater. Char.* 167 (2020), 110489, <https://doi.org/10.1016/j.matchar.2020.110489>.
- [70] J. Chen, Y. Yang, D. Wang, Z. Liu, C. Song, Effect of manufacturing steps on the interfacial defects of laser powder bed fusion 316L/CuSn10, *Mater. Lett.* 292 (2021), 129377, <https://doi.org/10.1016/j.matlet.2021.129377>.
- [71] A. Wegner, G. Witt, Konstruktionsregeln für das Laser-Sintern, *Zeitschrift Kunststofftechnik (Journal of Plastics Technology)* 8 (2012) 252–277.
- [72] G.A.O. Adam, Systematische Erarbeitung von Konstruktionsregeln für die additiven Fertigungsverfahren Lasersintern, Laserschmelzen und Fused Deposition Modeling, Dissertation, Forschungsberichte des Direct Manufacturing Research Centers, DMRC), 2015.
- [73] D. Thomas, The Development of Design Rules for Selective Laser Melting, Cardiff Metropolitan University, Dissertation, 2009, <https://doi.org/10.25401/cardiffmet.20974597.v1>.
- [74] R. Schäfer, Design Guidelines for Rapid Prototyping - Entwicklung von Konstruktionsrichtlinien für ein fertigungsgerechtes Gestalten anhand des Fused Deposition Modeling, Master's Thesis, Hochschule Bremen, 2008. <http://nbn-resolving.de/urn:nbn:de:gbv:46-dipl000001084>.
- [75] Deutsches Institut für Normung e. V., DIN 2275:2014-03 - Fühlerlehren, Beuth Verlag GmbH, Berlin, 2014.